ON THE USE OF SMOOTH VELOCITIES IN RAY-BASED STACKING AND TIME-MIGRATION

L.-J. Gelius and M. Tygel

email: *gelius@geo.uio.no and tygel@ime.unicamp.br*
keywords: *CRS, time migration, image ray, stacking*

ABSTRACT

We revisit ray-based approaches to stacking and time migration of seismic data, and investigate the role of the smooth-velocity condition normally attached to such techniques. It is demonstrated that the smooth velocity field plays the role of a replacement medium which ideally should have the following characteristic: the one-way analogues of the stacking and time-migration operators can be approximated in a paraxial sense by means of its impulse responses. In order to link the intrinsic properties of this smooth medium to the data-driven velocities, an incremental ray propagator system has been introduced. Based on this system, it is shown how stacking and time-migration velocities can be regarded as paraxial quantities which can be mapped to intrinsic properties representing information sampled along the central or mapping ray of the paraxial impulse responses considered.

INTRODUCTION

Extraction of stacking and time-migrating velocities from field data are routine procedures in seismic processing with the aim of producing reliable images and geological attributes from the subsurface. Because such (time-domain) velocities are directly estimated from the data, one may refer to them as data-driven velocities. A next, much more complicated task is to invert, from the data-driven velocities, corresponding depth-domain velocities, which somehow capture the intrinsic properties of the subsurface medium. Within acceptable limits, the inverted velocities must be such that: (a) The seismic wave propagation in depth honor the observed data; (b) the images produced with the help of the the inverted velocities are consistent with the available geological content of the illuminated subsurface. The construction of depth velocities with the above characteristics is a far from solved problem. An account of the state-of-the art approaches and results to velocity model building can be found in Jones (2010) with a comprehensive literature therein.

In the following, we use the imaging tool of time-to-depth conversion of time migration data, to gain a better insight to the concept and role of data-driven and depth velocities in that process. As it is the case of ray-based time migration approaches, our formulation assumes a smooth velocity medium in which the image-ray concept represents a valid mapping between time and depth. As established in Cameron et al. (2007), a key relation exists between time-migration velocities (i.e., data-driven velocities) and their corresponding smooth velocities in depth.

A more unified analysis is presented here, where both ray-based stacking and time-migration techniques are considered in a parallel manner. Smoothing of velocity fields is routinely applied in connection with both stacking and migration of seismic data. The construction of such fields is often rather ad hoc and mainly based on visual inspection and performance (e.g., enough smoothness to avoid apparently artificial events). We demonstrate that the ideal smooth velocity field associated with ray-based techniques can be regarded as a *replacement medium* with well-defined characteristics. Thus, not only the image-ray concept is valid, but also the normal-ray concept in case of stacked data. This implies that data-driven

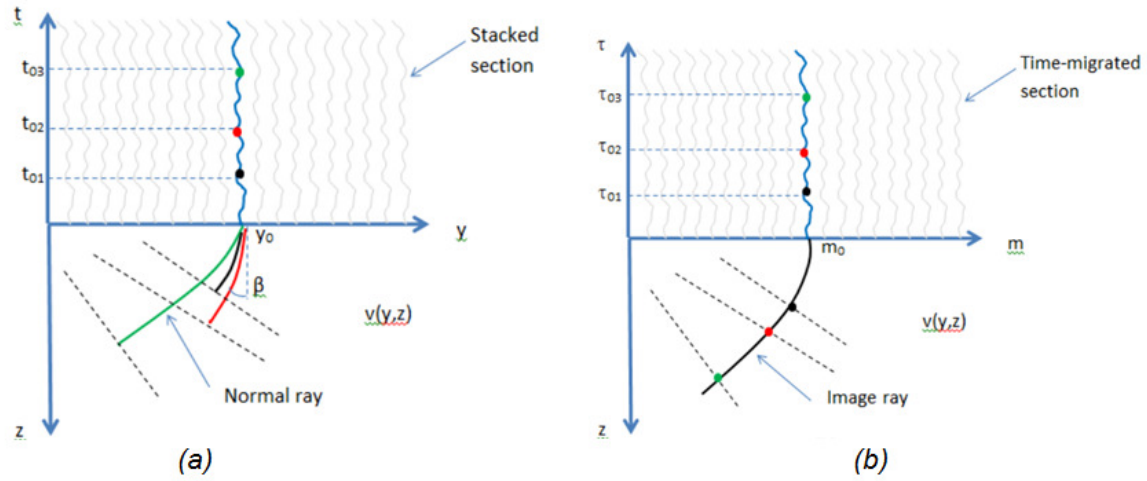

Figure 1: Time-to-depth mapping. (a) Stacked section and normal ray. (b) Time-migrated section and image ray.

velocities, such as NMO-velocities and time-migration velocities, are both ray-mapped to intrinsic properties (velocities) of the same smooth model. The mapping rays play the role of central rays of paraxial impulse responses associated with common scatterer points (CSP) in case of time-migration, and common reflection points (CRP) in case of stacking. These impulse responses are again closely linked to the corresponding operators of time migration and stacking. To properly describe the information content of a paraxial impulse response of a smooth medium, we introduce a special version of paraxial raytracing based on an *incremental ray-propagator system*.

SMOOTH VELOCITIES AND RAY-BASED APPROACHES TO STACKING AND TIME-MIGRATION

In this section we discuss ray-based approaches to stacking (e.g., Common Reflection Surface (CRS) technique (Jäger et al., 2001)) and time-migration (integral equation or Kirchhoff type (Schleicher et al., 2007)). For both techniques, smooth velocities are assumed, however without a clear understanding of what such velocities do represent. From velocity analysis, stacking velocities are obtained after smoothing of high-coherency velocity picks. However, such smoothing is carried out in a rather ad hoc manner. Similarly, migration velocities are typically derived from such smooth stacking velocities, with possible updating based on coherency measures. Again, the construction of the final smooth velocity field is designed by more or less subjective criteria.

In the analysis presented here, it will be clear what characteristics this smooth velocity field ideally should have. Moreover, it will be seen that this ideal field represents a replacement medium, in such a way that the stacking and migration operators are closely related to the paraxial impulse responses calculated along the corresponding time-to-depth mapping rays. In case of a stacked section, the mapping ray from time-to-depth is defined by the normal ray as shown in Fig.1a. In case of a time-migrated section, the mapping is governed by the image ray as shown in Fig.1b. In both cases, the velocity model is assumed smooth and equal. From the above understanding, it follows that stacking and time-migration velocities have much in common and are closely linked to the smooth velocity field. We will see that the underlying assumption is that the one-way version of the stacking and time-migration operators can be locally approximated by impulse responses, if the smooth or replacement velocity field is 'correctly' chosen. Thus, in case of stacking, there is an underlying assumption of a CRP scenario (cf. Fig.2a) and correspondingly, in case of time-migration, a CSP scenario (cf. Fig.2b).

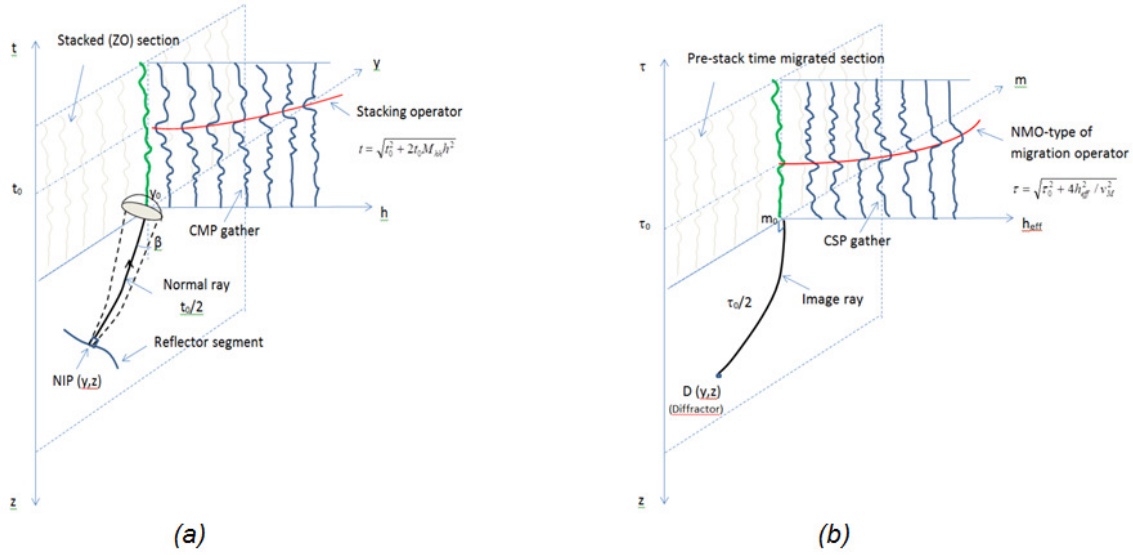

Figure 2: Paraxial-ray impulse description of (a) stacking operator and (b) time-migration operator.

Common Reflection Surface (CRS) stacking

In its simplest form, the Common Reflection Surface (CRS) method (see, e.g., Jäger et al., 2001) uses as stacking moveout the generalized hyperbolic traveltime in offset-midpoint (y, h) coordinates as a paraxial approximation around the (central) zero-offset (ZO) normal ray. In 2D, and assuming a straight seismic line, such moveout reads (t_0 is the two-way traveltime along the central ray and y_0 is the central midpoint)

$$t^2(y,h) = [t_0 + A(y-y_0)]^2 + B(y-y_0)^2 + Ch^2 \,, \tag{1}$$

with

$$A = \frac{2\sin\beta}{v_0}, \quad B = \frac{2t_0\cos^2\beta}{v_0 R_N}, \quad C = \frac{2t_0\cos^2\beta}{v_0 R_{NIP}} \,. \tag{2}$$

In equation (2), β is the take-off angle of the central/normal ray, v_0 is the surface velocity and R_{NIP} is the radius of curvature (paraxial sense) associated with a point source at the normal-incidence point (NIP) of the central ray at the reflector segment and measured at the surface in ray-centered coordinates. Similarly, R_N is the radius of curvature of a local exploding reflector wave initiated around the same NIP. Equation (1) can be interpreted as a paraxial approximation of a reflection traveltime surface that originates from a reflector element surrounding the NIP. By considering data sorted in common midpoint (CMP) gathers (i.e. with $y = y_0$), equation (1) reduces to the same form as the well-known normal moveout (NMO)-equation:

$$t^2(y=y_0,h) = t_0^2 + Ch^2 \,, \tag{3}$$

in which we readily relate the coefficient C to the NMO velocity, v_{NMO},

$$C = \frac{4}{v_{NMO}^2} \,. \tag{4}$$

Within the CRS formulation, equation (3) can be interpreted as a paraxial approximation of a reflection traveltime or NMO curve that originates from an unknown CRP (located at NIP). Alternatively, it can be interpreted as a diffraction curve associated with a scatterer at NIP. The point (y_0, t_0) specifies the apex of the NMO-curve. Thus, the normal ray that starts at the NIP hits the seismic line at y_0 and traveltime $t_0/2$. Equivalently, the normal ray that propagates backward in time hits the NIP when the (one-way) traveltime $t_0/2$ is consumed (cf. Fig.2a). Note also that the wavefront along the normal ray from NIP to y_0 makes an angle β with the seismic line. For each sample point (y_0, t_0), the parameter C can be determined from

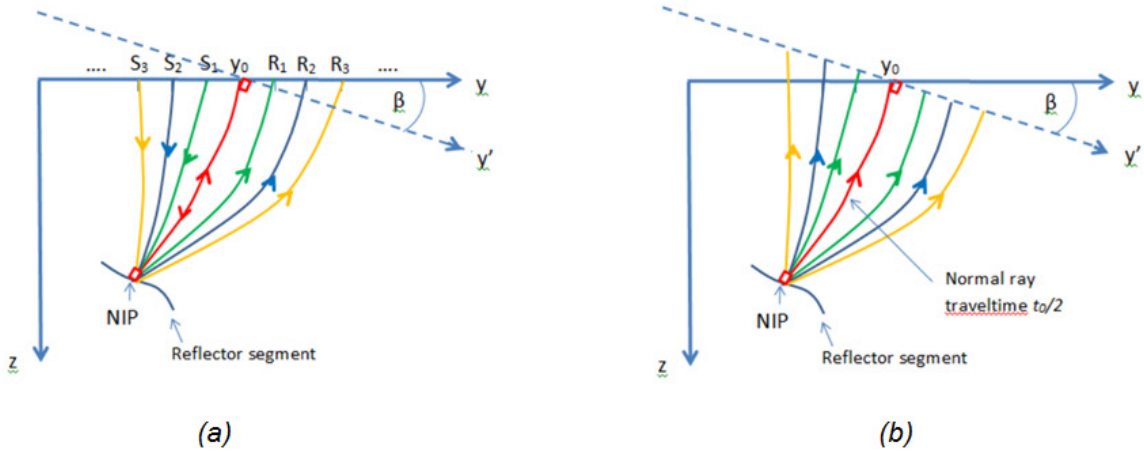

Figure 3: (a) Stacking operator and (b) its one-way analogy assuming reciprocity and local symmetry.

a two-step procedure: (i) a standard velocity analysis is first carried out to define guide functions (initial approximation of the velocity curve) and (ii) the guide functions with a user defined spread are then used to compute the $C = C(y_0, t_0)$ value at the given sample point. Note that, since there is an underlying paraxial approximation, *only smaller offsets should be considered*. Figure 3a shows schematics of the rays defining the local CRS stacking operator as approximated by a CRP response (i.e. ideal smooth velocity field). Note that the kinematics of this operator is based on two-way traveltimes. Its one-way traveltime equivalent can be approximated by the operator shown in Fig.3b, assuming reciprocity and local symmetry. Note, that the one-way traveltime now is measured along the new axis $y' = q$ (local ray coordinate), being perpendicular to the central ray at y_0. The kinematics of this one-way operator analogy of the stacking operator is governed by the equation (cf. equation (3) with the coordinate transformation $q = h\cos\beta$ and half traveltimes $T = t/2$ and $T_0 = t_0/2$):

$$T^2(y = y_0, q) = T_0^2 + \frac{C}{4\cos^2\beta}\, q^2 \,. \tag{5}$$

In the framework of Fig. 3b, and well known from ray theory, the time-wavefront curvature, $M_{NIP} = (v_0 R_{NIP})^{-1}$, satisfies the relationship

$$M_{NIP} = \left.\frac{d^2T}{dq^2}\right|_{q=0} \,. \tag{6}$$

As a consequence, twice differentiation of equation (5) with respect to q, and also use of equation (4) readily yields

$$M_{NIP} = \frac{C}{4T_0\cos^2\beta} = \frac{1}{T_0\, v_{NMO}^2\cos^2\beta} \,. \tag{7}$$

Prestack time migration

In the following, midpoint and half-offset coordinates in the time-migration domain will be denoted by (m, h). The two-way time-migrated traveltime is denoted τ. Of course, such coordinates will be always considered in the vicinity (paraxial) to the central midpoint and half-offset coordinates, m_0 and $h_0 = 0$, and central traveltime,τ_0. If one can assume that the time-migration velocity is offset independent (e.g., by using, in the migration, smaller offsets only), the moveout equation for prestack migration can be written as

$$\tau^2(m, h) = \tau_0^2 + \frac{4}{v_M^2}[(m - m_0)^2 + h^2] \,, \tag{8}$$

where $v_M = v_M(m_0, \tau_0)$ denotes the time-migration velocity. One possible implementation of equation (8) is to first introduce a so-called *asymptotic effective offset*, denoted by h_{eff} and given by

$$h_{eff}^2 = (m - m_0)^2 + h^2 \, , \tag{9}$$

which transforms the prestack time-migration moveout (8) into an NMO-like expression

$$\tau^2(m, h) = \tau_0^2 + \frac{4}{v_M^2} \, h_{eff}^2 \, . \tag{10}$$

This formulation can be regarded as an asymptotic version of the effective-offset approach to pre-stack migration denoted Equivalent Offset Migration (EOM) (Bancroft et al., 1994). To see that, EOM starts with the double-square-root (DSR) equation for migration (Yilmaz, 2001)

$$\tau(m, h) = \sqrt{\left\{ \frac{(m - m_0) - h}{v_M} \right\}^2 + \left(\frac{\tau_0}{2} \right)^2} + \sqrt{\left\{ \frac{(m - m_0) + h}{v_M} \right\}^2 + \left(\frac{\tau_0}{2} \right)^2} \, . \tag{11}$$

Squaring equation (11) twice and reorganizing, gives the alternative form (Li et al., 1997)

$$\tau^2(m, h) = \tau_0^2 + \frac{4}{v_M^2} \left[(m - m_0)^2 + h^2 \right] - \frac{4}{v_M^2} \, \frac{4(m - m_0)^2 h^2}{v_M^2 \tau^2(m, h)} \, . \tag{12}$$

The effective offset now takes the general form

$$h_{eff}^2 = (m - m_0)^2 + h^2 - \frac{4(m - m_0)^2 h^2}{v_M^2 \tau^2(m, h)} \, . \tag{13}$$

If we assume larger traveltimes the last term in equation (13) can be neglected, and the effective offset is given by its asymptotic representation. A practical implementation of equation (10) involves two steps: (i) mapping to effective-offset and (ii) followed by 'NMO-type' correction in the effective-offset domain. We will now briefly discuss in more detail how the mapping step can be implemented. At each location $m = m_0$ a so-called CSP gather is formed that will replace the classical CMP-gather associated with the same midpoint location. The spatial axis of a CSP-gather will be effective offset. Unlike the CMP-gather, which will be vulnerable to reflector dip (reflector smearing), the CSP-gather will ideally represent data from same scatterer locations (dip-moveout is inherent). Each CSP-gather is constructed from a family of CMP-gathers representing a range in midpoints from m_0 to m_{max}, with the latter being the migration aperture (cf. Fig.4). Each trace is only mapped along the spatial axis and the time-coordinate is not changed. Since this transformation is nonlinear, a binning procedure is applied along the effective offset axis. For each CSP-gather, multiple traces can be present at a given effective offset (fold). Such traces are stacked together and normalized with the fold. There is also a need to introduce an amplitude weight factor by analogy with Kirchhoff migration. Li et al. (1997) propose two different possible scale factors:

$$\text{scale}_1 = 1 - \frac{(m - m_0)}{h_{eff}} \quad \text{and} \quad \text{scale}_2 = 1 - \left(\frac{(m - m_0)}{h_{eff}} \right)^2 \, . \tag{14}$$

After all the CSP-gathers are constructed employing the mapping procedure, the final step involves a NMO-type of correction followed by stacking of each gather (cf. Fig.2b). This CSP-stacked section gives now the time-migrated result.

The migration operator associated with each CSP gather is defined by two-way travetime moveouts as governed by equation (10). By analogy with the CRS stacking case, we introduce the one-way traveltime equivalent, $\mathcal{T}(m, h) = \tau(m, h)/2$, of this operator, as described by Fig.5 in case of ZO (i.e. paraxial impulse response with secondary source at CSP and central ray equal to image ray)

$$\mathcal{T}^2(m, h) \equiv \frac{\tau^2(m, h)}{4} = \mathcal{T}_0^2 + \frac{1}{v_M^2} \, h_{eff}^2 \, . \tag{15}$$

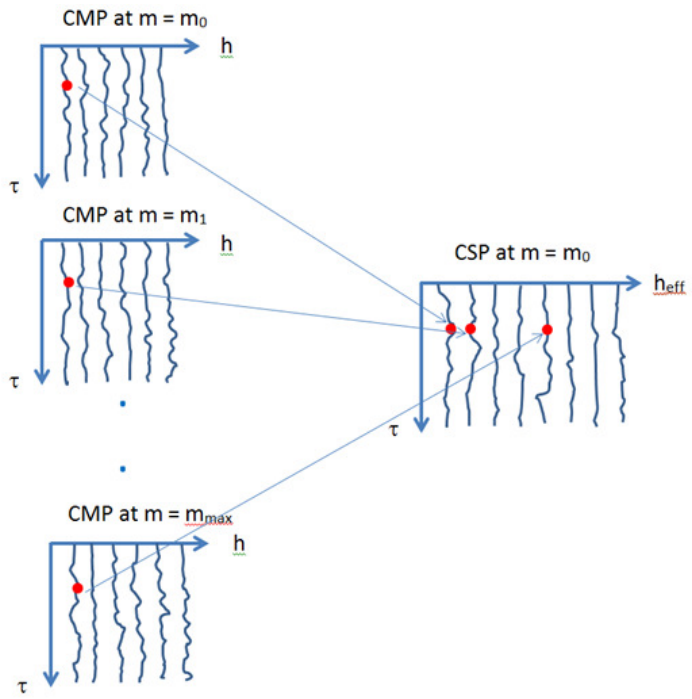

Figure 4: Mapping to effective offset: forming a CSP-gather from a family of CMP-gathers.

where $\mathcal{T}_0 = \tau_0/2$. The time-wavefront curvature associated with the moveout in equation (15) is given by

$$\mathcal{M} = \frac{d^2\mathcal{T}}{dh_{eff}^2}\bigg|_{h_{eff}=0} = \frac{1}{\mathcal{T}_0\, v_M^2}\,. \tag{16}$$

From equations (7) and (16), it readily follows that the scaled time-wavefront curvature of the paraxial impulse response of the smooth velocity medium is inversely proportional to the square of the data-driven velocities (i.e. stacking and time-migration velocities). The scale factor is equal to the one-way traveltime along the mapping (normal or image) ray. The additional angular factor present in equation (7) reflects the fact that the ray coordinate, q, makes an angle with the actual measurement (e.g. offset) axis. In order to unravel the link between the data driven velocities and that of the smooth medium, we need to establish an expression for the time-wavefront curvature associated with a paraxial impulse response of the smooth velocity model. This observation has motivated the development of the incremental ray propagator approach presented in the next main section.

However, before concluding this chapter, we also demonstrate how NMO (stacking) velocities and time-migration velocities are closely connected within a ray approach formulation.

Linking NMO-velocities to time-migration velocities

The 2D diffraction curve employed in time-migration (referred to as a time-migration stacking moveout) can also be formulated within a CRS parametrization. Consider Fig.6 which shows schematics of a ZO (stacked) section with a reflection response measured associated with an arbitrary reflector in depth together with the corresponding ZO time-migration operator. This reflection falls at sample t_0 for the trace with midpoint y_0. If this event is traced backward along the normal ray in the depth domain until the one-way traveltime $t_0/2$ is consumed, the local reflector segment will be orthogonal to the ray at this point (map migration). This termination point is denoted NIP (normal incidence point). From the CRS analysis it follows that at each data point (y_0, t_0) in the ZO section three parameters are estimated: A, B and C (cf. equation (1)). The question is now how to construct the corresponding diffraction response from knowledge of the CRS reflection response at (y_0, t_0). This operator will correspond to a point scatterer placed at NIP.

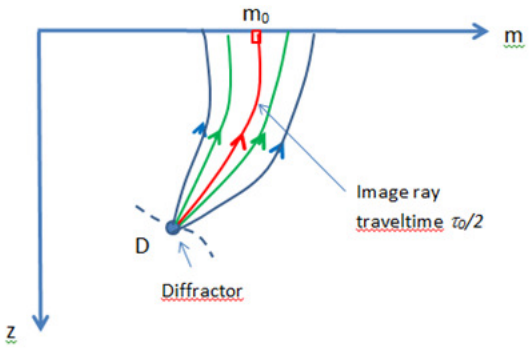

Figure 5: Interpretation of the one-way version of the time-migration operator as a paraxial-wave impulse response, with the image ray serving as the reference ray (ZO case or post-stack migration shown here).

Such a scatterer can be regarded as the limiting case when a reflector element shrinks to a point. This implies that $R_N = R_{NIP}$ or $B = C$. From equation (1) it then follows that this time diffraction operator can be written formally as (considering the prestack case and with offsets being not too large)

$$T^2(y,h) = [t_0 + A(y - y_0)]^2 + C[(y - y_0)^2 + h^2] \, . \tag{17}$$

In time migration we assume that the scatterer is located vertically in time below the current trace location being imaged. Let us denote this location m_0. We now assume prestack time migration employing the equivalent-offset approach, where the time-migration stacking curve is given by equation (10). The apex of this operator corresponds to $h_{eff} = 0$, which again implies $m = m_0$ and $h = 0$. Imposing this condition in equation (17) gives the following constraint

$$\left.\frac{dt}{dy}\right|_{y=m_0,h=0} \Rightarrow At_0 + A^2(m_0 - y_0) = 0 \Rightarrow m_0 = y_0 - \frac{A}{A^2 + C}\, t_0 \, . \tag{18}$$

Inserting equation (18) into equation (8) and equating equations (8) and (17) gives (also using equations (2) and (7))

$$v_M^2 = \left[\frac{1}{v_{NMO}^2} + \frac{\sin^2\beta}{v_0^2}\right]^{-1} \, , \tag{19}$$

and

$$\tau_0^2 = t_0^2 - \left(\frac{v_M t_0 \sin\beta}{v_0}\right)^2 \, . \tag{20}$$

where $v_M = v_M(m_0, \tau_0)$, $\beta = \beta(y_0, t_0)$ and $v_{NMO} = v_{NMO}(y_0, t_0)$. Based on equation (20), we can revise equation (18) as follows

$$m_0 = y_0 - \frac{v_M^2 t_0 \sin\beta}{2v_0} \, . \tag{21}$$

Similar expressions have been derived earlier by Mann et al. (2000) considering the ZO limit but using a slightly different parametrization (R_{NIP} instead of v_{NMO}). We think that the mapping formulation introduced here gives a clearer idea of how NMO-velocities and time-migration velocities relate.

In case of a stratigraphic earth model ($\beta = 0$), it follows from equation (19) that

$$v_M(m_0, \tau_0) = v_M(y_0, t_0) = v_{NMO}(y_0, t_0) \quad [= v_{RMS}(y_0, t_0)] \, . \tag{22}$$

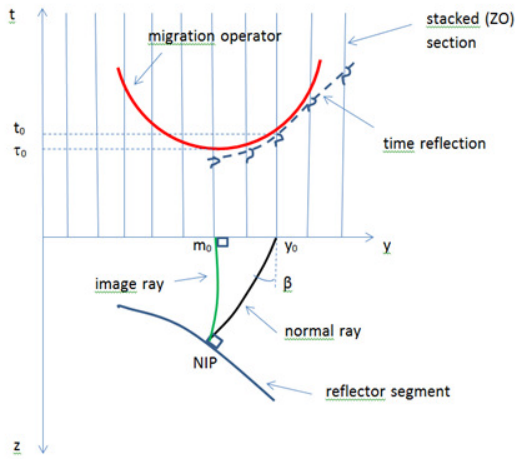

Figure 6: Mapping from stacking domain to time-migration domain (post-stack migration case shown here).

THE 2-D INCREMENTAL RAY PROPAGATOR

In this section, a naive approach to paraxial raytracing in a 2-D model is derived. The overall goal is to obtain simple analytical expressions describing the main characteristics of the impulse response of a smooth velocity model. By means of such information, we can link the data-driven velocities to intrinsic properties of the smooth velocity field (replacement field).

Incremental tracing

The starting point is the paraxial dynamic ray-tracing system in ray-centered coordinates, which in a 2D medium reads (Červený, 2001)

$$\frac{dQ}{dT} = v^2\, P, \quad \frac{dP}{dT} = -v^{-1} v_{qq}\, Q\ , \tag{23}$$

where T is the traveltime along the central ray, v is the medium velocity (measured along the central or reference ray) and v_{qq} is the second derivative of the velocity with respect to the ray centered coordinate q (i.e. along a direction orthogonal to the central ray direction). Taking the time derivative of the above two equations gives

$$\begin{aligned} \frac{d^2Q}{dT^2} &= 2v\,\frac{dv}{dT}\,P + v^2\,\frac{dP}{dT} = 2v\,\frac{dv}{dT}\,P - v\,v_{qq}\,Q\ , \\ \frac{d^2P}{dT^2} &= -\frac{d}{dT}\left(v^{-1}v_{qq}\right)Q - v^{-1}v_{qq}\frac{dQ}{dT} = -v^{-1}v_{qq}\frac{d\ln\left(v^{-1}v_{qq}\right)}{dT}\,Q - v\,v_{qq}\,P\ . \end{aligned} \tag{24}$$

Consider now two nearby points $\mathbf{x}_i$ and $\mathbf{x}_{i+1}$ (not end points) along the central ray representing an incremental traveltime difference δT (cf. Fig.7) and introduce the following Taylor expansions to second order in traveltime (employing the notation $Q_i \equiv Q(\mathbf{x}_i)$ and similarly for P_i, v_i and $v_{i,qq}$)

$$\begin{aligned} Q_{i+1} &\cong Q_i + \frac{dQ_i}{dT}\,\delta T + \frac{1}{2}\frac{d^2Q_i}{dT^2}\,\delta T^2 = \left(1 - \frac{1}{2}v_i\,v_{i,qq}\,\delta T^2\right)Q_i + (v_i^2\delta T)P_i\ , \\ P_{i+1} &\cong P_i + \frac{dP_i}{dT}\,\delta T + \frac{1}{2}\frac{d^2P_i}{dT^2}\,\delta T^2 = [-v_i^{-1}v_{i,qq}\delta T]Q_i + \left(1 - \frac{1}{2}v_i\,v_{i,qq}\,\delta T^2\right)P_i\ . \end{aligned} \tag{25}$$

In equation (25) we have neglected the time derivatives in equation (24) and assumed constant values within each time step. As usual practice, the system in equation (25) can be conveniently recast in matrix form

$$\begin{bmatrix} Q_{i+1} \\ P_{i+1} \end{bmatrix} = {}_{\uparrow}\Delta\pi_i \begin{bmatrix} Q_i \\ P_i \end{bmatrix} , \tag{26}$$

where ${}_{\uparrow}\Delta\pi_i$ is the ray-propagator matrix along the incremental ray segment from $\mathbf{x}_i$ to $\mathbf{x}_{i+1}$, given by

$${}_{\uparrow}\Delta\pi_i = \begin{bmatrix} {}_{\uparrow}\Delta Q_1 & {}_{\uparrow}\Delta Q_2 \\ {}_{\uparrow}\Delta P_1 & {}_{\uparrow}\Delta P_2 \end{bmatrix} = \begin{bmatrix} 1 - \frac{1}{2} v_i \, v_{i,qq} \delta T^2 & v_i^2 \, \delta T \\ -v_i^{-1} v_{i,qq} \delta T & 1 - \frac{1}{2} v_i \, v_{i,qq} \delta T^2 \end{bmatrix} . \tag{27}$$

In analogy with the usual definition of the propagator matrix (Červený, 2001), the columns $({}_{\uparrow}\Delta Q_1, {}_{\uparrow}\Delta P_1)^T$ and $({}_{\uparrow}\Delta Q_2, {}_{\uparrow}\Delta P_2)^T$ of the matrix ${}_{\uparrow}\Delta\pi_i$ represent the incremental plane-wave (telescopic) and point-source solutions of the dynamical ray-tracing system along the incremental ray that connect the nearby points $\mathbf{x}_i$ and $\mathbf{x}_{i+1}$. In the same way, ${}_{\uparrow}\Delta\pi_i$ fulfills the symplectic condition (Červený, 2001) (within 2nd order time perturbation)

$$({}_{\uparrow}\Delta\pi_i) \, J \, ({}_{\uparrow}\Delta\pi_i)^T = J , \quad \text{with} \quad J = \begin{bmatrix} 0 & 1 \\ -1 & 0 \end{bmatrix} \tag{28}$$

from which $|{}_{\uparrow}\Delta\pi_i| = 1$.

The time-reversed version of equation (26) will formally read

$$\begin{bmatrix} Q_i \\ P_i \end{bmatrix} = ({}_{\uparrow}\Delta\pi_i)^{-1} \begin{bmatrix} Q_{i+1} \\ P_{i+1} \end{bmatrix} \equiv ({}_{\downarrow}\Delta\pi_i) \begin{bmatrix} Q_{i+1} \\ P_{i+1} \end{bmatrix} \tag{29}$$

Note that the equality between the inverse and the time-reversed incremental ray propagator holds because we are not considering the complete ray propagation from source to receiver. From the symplectic condition, together with the definition of the ray centered coordinates, we have (Červený, 2001)

$${}_{\downarrow}\Delta\pi_i = ({}_{\uparrow}\Delta\pi_i)^{-1} = J^T ({}_{\uparrow}\Delta\pi_i)^T J = \begin{bmatrix} {}_{\downarrow}\Delta Q_1 & {}_{\downarrow}\Delta Q_2 \\ {}_{\downarrow}\Delta P_1 & {}_{\downarrow}\Delta P_2 \end{bmatrix} = \begin{bmatrix} {}_{\uparrow}\Delta P_2 & -{}_{\uparrow}\Delta Q_2 \\ -{}_{\uparrow}\Delta P_1 & {}_{\uparrow}\Delta Q_1 \end{bmatrix} . \tag{30}$$

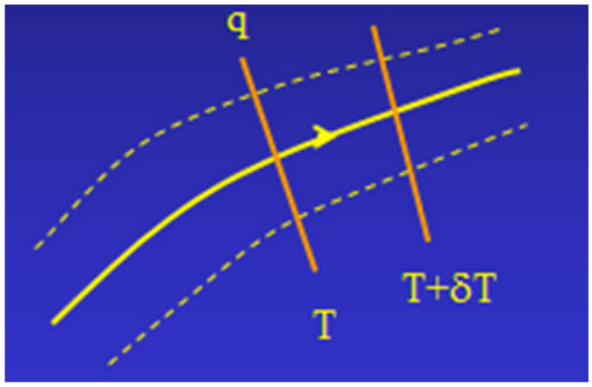

Figure 7: Incremental paraxial raytracing.

Cascaded system

Based on equations (26) and (27), corresponding cascaded solutions can be constructed. Assume a total of N time steps (corresponding to a total traveltime $T = N\delta T$). Then we can write, in case of forward propagation in time (assuming either point or telescopic source initial condition),

$$\begin{bmatrix} {}_{\uparrow}Q_{fin} \\ {}_{\uparrow}P_{fin} \end{bmatrix} = ({}_{\uparrow}\Delta\pi_N) \cdots ({}_{\uparrow}\Delta\pi_2)({}_{\uparrow}\Delta\pi_1) \begin{bmatrix} {}_{\uparrow}Q_{ini} \\ {}_{\uparrow}P_{ini} \end{bmatrix} = {}_{\uparrow}\pi \begin{bmatrix} {}_{\uparrow}Q_{ini} \\ {}_{\uparrow}P_{ini} \end{bmatrix} , \tag{31}$$

where ${}_{\uparrow}\pi$ represents the ray-propagator matrix along the full ray

$$ {}_{\uparrow}\pi = ({}_{\uparrow}\Delta\pi_N)\cdots({}_{\uparrow}\Delta\pi_2)({}_{\uparrow}\Delta\pi_1) = \begin{bmatrix} {}_{\uparrow}Q_1 & {}_{\uparrow}Q_2 \\ {}_{\uparrow}P_1 & {}_{\uparrow}P_2 \end{bmatrix} \tag{32} $$

The telescopic and point-source components of the propagator matrix are found to be

$$ \begin{aligned} {}_{\uparrow}Q_1 &= 1 - \sum_{i=1}^{N} \left\{ \sum_{k=1}^{N} v_k^2\,\delta T - \frac{3v_i^2\delta T}{2} \right\} v_i^{-1}\, v_{i,qq}\,\delta T\,, \\ {}_{\uparrow}P_1 &= -\sum_{i=1}^{N} v_i^{-1}\, v_{i,qq}\,\delta T\,, \\ {}_{\uparrow}Q_2 &= \sum_{i=1}^{N} v_i^2\,\delta T\,, \\ {}_{\uparrow}P_2 &= 1 - \sum_{i=1}^{N} \left\{ \sum_{k=1}^{N} v_k^2\,\delta T - \frac{3v_i^2\,\delta T}{2} \right\} v_i^{-1}\, v_{i,qq}\,\delta T\,, \end{aligned} \tag{33} $$

The corresponding cascaded system in case of time-reversed propagation reads

$$ \begin{aligned} \begin{bmatrix} {}_{\downarrow}Q_{fin} \\ {}_{\downarrow}P_{fin} \end{bmatrix} &= ({}_{\downarrow}\Delta\pi_1)({}_{\downarrow}\Delta\pi_2)\cdots({}_{\downarrow}\Delta\pi_{N-1})({}_{\downarrow}\Delta\pi_N) \begin{bmatrix} {}_{\downarrow}Q_{ini} \\ {}_{\downarrow}P_{ini} \end{bmatrix} \\ &= J^T({}_{\uparrow}\Delta\pi_1)^T({}_{\uparrow}\Delta\pi_2)^T\cdots({}_{\uparrow}\Delta\pi_{N-1})^T({}_{\uparrow}\Delta\pi_N)^T J \begin{bmatrix} {}_{\downarrow}Q_{ini} \\ {}_{\downarrow}P_{ini} \end{bmatrix} \\ &= \left(J^T\,{}_{\uparrow}\pi\, J\right)^T \begin{bmatrix} {}_{\downarrow}Q_{ini} \\ {}_{\downarrow}P_{ini} \end{bmatrix} = {}_{\downarrow}\pi \begin{bmatrix} {}_{\downarrow}Q_{ini} \\ {}_{\downarrow}P_{ini} \end{bmatrix}\,. \end{aligned} \tag{34} $$

which, in combination with equation (31), gives the well-known relationships between forward and reverse time-propagated ray matrices (by analogy with equation (30)) (Červený, 2001)

$$ \begin{aligned} {}_{\downarrow}\pi &= \begin{bmatrix} {}_{\downarrow}Q_1 & {}_{\downarrow}Q_2 \\ {}_{\downarrow}P_1 & {}_{\downarrow}P_2 \end{bmatrix} = J^T({}_{\uparrow}\pi)^T J \\ &= J^T \begin{bmatrix} {}_{\uparrow}Q_1 & {}_{\uparrow}Q_2 \\ {}_{\uparrow}P_1 & {}_{\uparrow}P_2 \end{bmatrix}^T J = \begin{bmatrix} {}_{\uparrow}P_2 & -{}_{\uparrow}Q_2 \\ -{}_{\uparrow}P_1 & {}_{\uparrow}Q_1 \end{bmatrix}\,. \end{aligned} \tag{35} $$

It follows from equation (35) that, if the dynamic quantities, Q and P, of the forward propagation in time are known, the corresponding quantities for the reverse time solution can be easily deduced (and vice versa). The forward-propagated solutions represent physical responses. Nevertheless, as later demonstrated, indirect quantities, such as the wavefront curvature (or its inverse), of the non-physical, time-reversed telescopic solutions can provide useful information about the local (interval) velocities. As a consequence, such solutions are bound to play an important role in velocity mapping, where the transformation is represented by tracing along normal or image rays. We observe, in passing, that these types of rays are telescopic in nature in a paraxial sense, since the wavefront is linear at the takeoff for an image ray (traced backward in time) and linear at the reflector for a normal ray (traced forward in time.

Special case of smooth velocity model

Consider now the special case of a smooth velocity model. This type of assumption is commonly employed both in stacking and migration of seismic data as discussed earlier. As demonstrated then, both the stacking and migration operators within a ray-based approach are closely related to the impulse response of such a smooth medium. Moreover, this smooth velocity field is not representing the true velocities of the subsurface but plays the role of a replacement medium. By imposing a smooth velocity condition, equations (33)

take the form

$$
\begin{aligned}
{}_{\uparrow}Q_1 &\cong 1 - T^2 v_{RMS}^2(0,T)\langle v^{-1}\, v_{qq}\rangle + T\langle v^{-1}\, v_{qq}\rangle_w \ , \\
{}_{\uparrow}P_1 &\cong -T\langle v^{-1}\, v_{qq}\rangle \ , \\
{}_{\uparrow}Q_2 &\cong T\, v_{RMS}^2 \ , \\
{}_{\uparrow}P_2 &= 1 - T\langle v^{-1}\, v_{qq}\rangle_w \ ,
\end{aligned}
\tag{36}
$$

in which we have employed the time averages

$$
\begin{aligned}
\langle v^{-1}\, v_{qq}\rangle &= \frac{1}{T}\int_0^T v^{-1}(T')\, v_{qq}(T')\, dT' \ , \\
\langle v^{-1}\, v_{qq}\rangle_w &= \frac{1}{T}\int_0^T T'\, v_{RMS}^2(0,T')\, v^{-1}(T')\, v_{qq}(T')\, dT' \ .
\end{aligned}
\tag{37}
$$

In equations (36), the notation $v_{RMS}(T_a, T_b)$ implies an RMS-velocity calculated along the central ray between propagation times T_a and T_b. We also adopted the simplifying notation $v_{RMS}(0,T) = v_{RMS}$.

RELATIONSHIP BETWEEN THE DATA DRIVEN VELOCITIES (TIME-WAVEFRONT CURVATURES) AND THE INTRINSIC PROPERTIES OF THE SMOOTH VELOCITY MODEL

We start by summarizing the main observations made up to now:

- Time-wavefront curvature of paraxial impulse response of smooth velocity model describes one-way version of ray-based operator for both stacking and time-migration.
- Application of operators to data determines time-wavefront curvatures (maximizing coherency measures).
- To link time-wavefront curvatures or data driven velocities ('observations') to intrinsic medium properties, need to compute paraxial impulse response of such a smooth medium.

Recovering intrinsic properties

The paraxial impulse response is calculated from equations (31) and (32) with propagation matrices corresponding to the smooth model as given by equations (36) and the following initial condition (v_i being the local or interval velocity at the source location):

$$
Q_{ini} = 0, \quad P_{ini} = \frac{1}{v_i} \ . \tag{38}
$$

Since the incremental raytracing system is calculated in local ray-coordinates, we use a subscript q on each quantity defined, as a reminder. If M_q represents the time-wavefront curvature of a paraxial impulse response of the smooth velocity model, we define the following 'observables' (i.e. determined from data employing appropriate operators and coherency criteria):

- Paraxial NMO-velocity:
$$
v_{qNMO}^2 = (T\, M_q)^{-1} \tag{39}
$$
- Paraxial Dix-velocity:
$$
v_{qDix}^2 = dM_q^{-1}/dT \ , \tag{40}
$$

where T represents the (one-way) traveltime along the central or mapping ray.

In the limit of infinitesimal time stepping and smooth model, the following main result was obtained from the incremental raytracing system

$$
M_q = \left.\frac{d^2T}{dq^2}\right|_{q=0} = \left(T\, v_{qRMS}^2\right)^{-1} .\aleph \equiv \left(T\, v_{qNMO}^2\right)^{-1} \ , \tag{41}
$$

with

$$v_{qRMS}^2 = \frac{1}{T}\int_0^T v^2(T')\,dT' \,, \qquad \aleph = 1 - \int_0^T T' v_{qRMS}^2(0,T')\,v^{-1}(T')\,v_{qq}(T')\,dT' \,. \tag{42}$$

In equation (42), v_{qRMS} represents the RMS-velocity calculated along the central or mapping ray and $\aleph$ is a stretch factor. Based on equations (41) and (42) and from knowledge of the wavefront-curvature, the intrinsic properties of the smooth velocity model (i.e. local velocity v) can be recovered as follows:

$$v = \sqrt{\frac{d\left(T\,v_{qRMS}^2\right)}{dT}} \,, \qquad v_{qRMS}^2 = v_{qNMO}^2.\aleph \,, \tag{43}$$

if the stretch factor is known. Hence, both in case of ray-based stacking and time-migration, the data-driven velocities determined (i.e., represented by time-wavefront curvature in equations (7) and (16)) can now be linked to the local intrinsic velocity, v.

Cameron et al. (2007) were the first to link time-migration velocities to the intrinsic properties of the smooth velocity model. The work presented here represents a more generalized approach to the same problem, by considering ray-based stacking and time-migration within a unified approach. Thus, a more complete understanding of data-driven velocities in general and their link to intrinsic properties are obtained. The unified approach also makes it clear what ideal characteristics the smooth velocity field should have (i.e. underlying paraxial assumptions). The main task has been to unravel the close relationship between the paraxial impulse response in the smooth medium and the corresponding stacking and migration operators. The impulse responses are paraxial approximations with the proper mapping rays acting as the central rays. In this paper, the concept of incremental ray propagator has been introduced. In their work, Cameron et al. (2007) employed a different solution strategy based on a perturbed-source approach (cf. Fig.8). In case of time-migration they arrived upon the main result

$$v^2 = \frac{d\left(M^{-1}\right)}{dT}.\aleph^2 = \frac{d\left(T\,v_{qNMO}^2\right)}{dT} \equiv v_{qDix}^2.\aleph \,, \tag{44}$$

Thus, they used the paraxial Dix-type of velocity as data input to estimate the local velocity. This involves the use of a time-differentiated time-wavefront curvature.

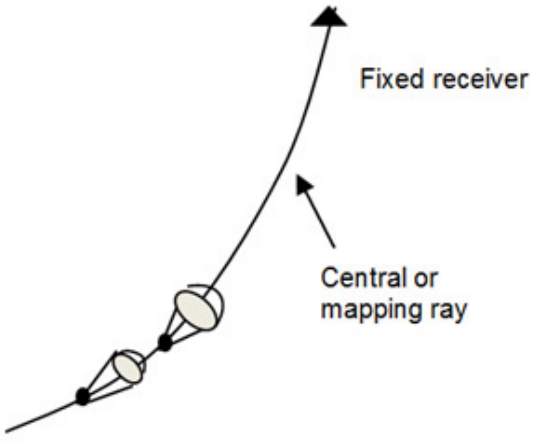

Figure 8: Perturbed-source approach employed to analyze intrinsic mapping.

When mapping data driven velocities (or time-wavefront curvatures) to intrinsic properties the following observation can be made: we measure quantities in a paraxial sense but want to transform them to quantities describing central ray (intrinsic properties, cf. Table1).

Paraxial-sense quantity	Central/mapping-ray quantity (intrinsic)
NMO-velocity: $v^2_{qNMO} = M^{-1}/T$	$v^2_{qRMS} = v^2_{qNMO}.\aleph, \quad v = \sqrt{d\left(T\, v^2_{qRMS}\right)/dT}$
Dix velocity: $v^2_{qDix} = d\left(M^{-1}\right)/dT$	$v^2 = v^2_{qDix}.\aleph$

Table 1: Mapping to intrinsic properties.

The stretch factor

The stretch factor $\aleph$ in equation (42) can be computed from time-reversed paraxial raytracing along the mapping rays employing a telescopic solution (Cameron et al., 2007). The time-reversed version of the incremental raytracing system is given by equations (34) and (35). From this system it readily follows that

$$ {}_{\downarrow}Q_1 = {}_{\uparrow}P_2 = v_0.\aleph \, . \tag{45}$$

Equation (45) gives an alternative interpretation of the stretch factor, namely that it is proportional to the geometrical spreading factor, $\mathcal{G} = {}_{\downarrow}Q_1$, of a telescopic paraxial ray computed backward in time along the mapping ray acting as the central ray. Figure 9 shows an example of such a ray tracing in case of an image ray.

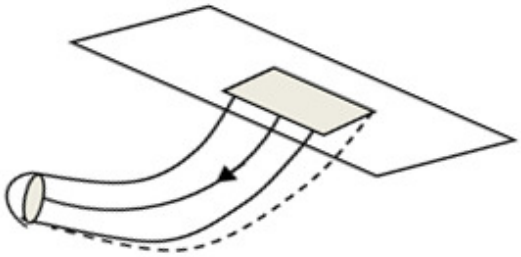

Figure 9: Time-reversed tracing of telescopic solution along image ray as its central ray.

We can now summarize the role of the elementary paraxial solution of the smooth velocity model:

- Paraxial point-source (impulse response) solution: links the paraxial type of velocity information (time-wavefront curvatures) to intrinsic quantities (e.g. local time-domain velocities).
- Time-reversed telescopic solution:
  - estimates stretch factor
  - provides mapping from time-to-depth.

Time-to-depth mapping

In the original work of Cameron et al. (2007), time-to-depth mapping of data-driven velocities to smooth intrinsic velocities in depth was the main goal. They suggested to solve for stretch factor and time-to-depth mapping jointly through inversion. Possible problems with this strategy can be:

- The quantity M at each sample has to be estimated from the data. One has to have 'reliable' estimates so as to compute dM/dT at every sample point;
- Estimates of M can be only trusted at points of high coherency;
- Instability can be expected.

An alternative strategy could be to decouple the problem:

- Use smooth macro-velocity field in depth obtained from tomography to estimate stretch and time-to-depth mapping
- Use only reliable values of M (samples with high-coherency) followed by 'smart' interpolation and time differentiation to recover v.

CONCLUSIONS

An incremental ray-propagator system has been introduced as a possible tool to more easily analyze the medium information carried by different elementary earth responses (point and telescopic type). This system is not to be regarded as a practical paraxial ray-tracing system, but serves the purpose of an analyzing tool. The concept is also well tailored for analyzing the so-called velocity stretch problem, i.e. how to recover local (interval) velocities from either time-migration or stacking velocities. Finally it should be noted that the generalization to the 3D case is rather straightforward.

ACKNOWLEDGMENTS

This work was kindly supported by the sponsors of the *Wave Inversion Technology (WIT) Consortium*, Karlsruhe, Germany.

REFERENCES

Bancroft, J. C., Geiger, H. D., Foltinek, D., and Wang, S. (1994). Prestack migration by equivalent offsets and CSP gathers. In *CREWES Research Report*, volume 6.

Cameron, M. K., Fomel, S. B., and Sethian, J. A. (2007). Seismic velocity estimation from time migration. *Inverse Problems*, 23:1329–1369.

Červený, V. (2001). *Seismic Ray Theory*. Cambridge University Press.

Jäger, R., Mann, J., Höcht, G., and Hubral, P. (2001). Common-reflection-surface stack: Image and attributes. *Geophysics*, 66(1):97–109.

Jones, I. (2010). *An Introduction to Velocity Model Building*. European Association of Geophysicists and Engineers (EAGE).

Li, X., Xu, Y., and Bancroft, J. (1997). Equivalent offset migration: the implementation and application update. In *CREWES Research Report*, volume 9.

Mann, J., Hubral, P., Traub, B., Gerst, A., and Meyer, H. (2000). Macro-model independent approximative prestack time migration. In *Extended Abstracts: 62nd Mtg. Eur. Assn. Geosci. Eng. (EAGE), Session B-52*, volume 6.

Schleicher, J., Tygel, M., and Hubral, P. (2007). *Seismic True Amplitudes*. SEG, Tulsa, USA.

Yilmaz, O. (2001). *Seismic Data Analysis: Processing, Inversion and Interpretation of Seismic Data (2nd edition)*. Society of Exploration Geophysicists (SEG), Oklahoma, Tulsa, USA.